CMOS Active Pixel Sensors as energy-range detectors for proton Computed Tomography

M. Esposito[a,b,1], **T. Anaxagoras**[c], **P.M. Evans**[b], **S. Green**[d,e], **S. Manolopoulos**[f], **J. Nieto-Camero**[g], **D.J. Parker**[d], **G. Poludniowski**[b], **T. Price**[d], **C. Waltham**[a], and **N.M. Allinson**[a]

[a]School of Computer Science, University of Lincoln, Lincoln, LN6 7TS, U.K.

[b]Centre for Vision, Speech and Signal Processing, University of Surrey, Guildford GU2 7XH, U.K.

[c]ISDI Ltd (Image Sensor Design and Innovation), Oxford, OX4 1YZ, U.K.

[d]School of Physics and Astronomy, University of Birmingham, Birmingham, B152TT, U.K.

[e]Hall Edwards Radiotherapy Research Group, University Hospital Birmingham NHS Foundation Trust, Birmingham, B15 2TH, U.K.

[f]University Hospitals Coventry and Warwickshire NHS Trust, Coventry, CV2 2DX, U.K.

[g]iThemba LABS, PO Box 722, Somerset West 7129, S.A.

Abstract

Since the first proof of concept in the early 70s, a number of technologies has been proposed to perform proton CT (pCT), as a means of mapping tissue stopping power for accurate treatment planning in proton therapy. Previous prototypes of energy-range detectors for pCT have been mainly based on the use of scintillator-based calorimeters, to measure proton residual energy after passing through the patient. However, such an approach is limited by the need for only a single proton passing through the energy-range detector in a read-out cycle. A novel approach to this problem could be the use of pixelated detectors, where the independent read-out of each pixel allows to measure simultaneously the residual energy of a number of protons in the same read-out cycle, facilitating a faster and more efficient pCT scan.

This paper investigates the suitability of CMOS Active Pixel Sensors (APSs) to track individual protons as they go through a number of CMOS layers, forming an energy-range telescope. Measurements performed at the iThemba Laboratories will be presented and analysed in terms of correlation, to confirm capability of proton tracking for CMOS APSs.

Keywords

Instrumentation for hadron therapy; Solid state detectors; Computerized Tomography (CT) and Computed Radiography (CR); Detector modelling and simulations I (interaction of radiation with matter, interaction of photons with matter, interaction of hadrons with matter, etc)

---

[1]Corresponding author. m.esposito@physics.org.

1 Introduction

Proton therapy is gaining importance in the field of radiotherapy, because of its potential of delivering the planned dose over a small depth range, defined and controlled by the proton energy, while relatively sparing surrounding healthy tissues [1]. The use of proton therapy for cancer treatment creates the need to develop new and more accurate imaging modalities for treatment planning, based on direct measurements of tissue stopping power instead of tissue density, as in conventional X-ray Computed Tomography (CT), to reduce the error in converting the latter quantity into the former [2].

Since the first proof of concept in the early 70s, a number of technologies have been proposed to perform proton CT (pCT), as a means of mapping tissues stopping power for an accurate treatment planning. The basic requirements for pCT lie in measuring position and direction of individual protons and assessing their residual energy after passing through the patient in an energy discriminating detector, in order to infer the most likely path in the patient of each proton and its deposited energy, thus the stopping power, along the inferred path.

Previous prototypes of energy-range detectors for pCT, have been chiefly based on the use of scintillator-based calorimeters [3–6], to measure proton residual energy. However, such an approach is limited by the need for only a single proton passing through the energy-range detector in a read-out cycle.

A novel approach to this problem is the use of pixelated detectors, where the independent read-out of each pixel allows to simultaneous measurement of the residual energy of a number of protons in the same read-out cycle, facilitating a faster and more efficient pCT scan. The Proton Radiotherapy Verification and Dosimetry Application (PRaVDA, Wellcome) [7] consortium is developing a pCT system based on the use of Silicon Strip Detectors (SSDs) as trackers [8], to provide the protons most likely path through the patient, and CMOS Active Pixel Sensors (APSs) used as an energy-range telescope, to infer residual proton energy by measuring the position where the proton stops in the telescope. A schematic representation of the proposed PRaVDA system is shown in figure 1.

A first proof of concept into the proton counting capability of CMOS APSs has been provided in [9]. This paper focuses on the investigation of the suitability of CMOS APSs to track individual protons as they pass through a number of CMOS wafers that forms the energy-range telescope. In fact, for residual proton energy to be reconstructed, proton tracks need to be reconstructed through the range telescope. In order to study the feasibility of proton tracking in a CMOS range telescope (RT), a simple telescope made from two stacked CMOS sensors was used. A study of the correlation between protons detected in the first and in the second detector of this simple RT, a condition necessary to perform proton tracking, is reported in this paper.

2 Materials and methods

2.1 The iThemba proton beam facility

The experimental work described in this paper was performed at the iThemba Laboratories (Cape Town, SA), a facility actively used for patient treatment. The maximum beam energy available at this facility is 191 MeV, corresponding to a range at the patient position, or iso-centre, of 240 ± 0.4 mm with a FWHM of 24 ± 1.0 mm (measured as 50% of maximum dose on the distal side of the Bragg peak in water). The wide-area beam (10 cm diameter) is achieved by using a system of passive scattering components and collimators, while the beam energy can be degraded by graphite attenuators. In the proton therapy beam set-up, the current range achievable at this facility is in the range 0.1-100 nA (measured at the exit of the vacuum beam line), however, for the purposes of the experiments reported in this paper, a different set-up was used making available lower currents. The iThemba physics research injector cyclotron was used with an external ion source, allowing copper filters, featuring evenly spaced holes, to be used further reducing the beam current. Those filters produce a reduction in beam current of a nominal factor of 10^{-2} or 10^{-4}.

2.2 Double DynAMITe detector

The DynAMITe CMOS APS [10, 11], an imaging detector designed for bio-medical applications, was used for the experiments described in this paper. DynAMITe was fabricated in a standard, incorporating radiation hardness by design, 0.18 μm CMOS technology using reticle stitching [12], covering a total active area of 12.8×13.1 cm^2. The smallest pixel size offered by this detector (50 μm) was used in this work.

A stack of two DynAMITe detectors placed one after the other was realised, in order to provide a simple two-layer range telescope as proof of principle of the PRaVDA range telescope. A picture showing the DD set-up at iThemba is given in figure 2(a). A minimum detector-to-detector distance of 10 mm was achievable, given the size of the electronic boards of the two detectors, and each detector features a 5 mm thick Al back-plate (see figure 2(b)). It is of note that the thickness of the Al plate after the first detector, represent a challenge for proton tracking, as this will provide additional material for protons to scatter in. Also, due to geometrical constraints, the two detectors are flipped (180 degree rotation in the image plane) with respect to each other. Furthermore, precise alignment as not possible for the two detectors, so that calibration of the relative misalignment had to be performed, by using high current beams and aligning the beam profiles in both detectors.

The readout of the two detectors was synchronised in order to allow for proton tracking, so that images were acquired simultaneously for both detectors. The same master clock, which is the basic timing signal for detector operations such as exposure, reset and readout, was provided to both detectors guaranteeing synchronous operations.

This configuration, using the two detectors stacked, is referred in this work as *Double DynA-MITe* (DD).

2.3 Experimental parameters

Several experimental parameters, such as beam energy, current, size, exposure time, were varied for the experiments described in this paper. Before introducing them tabularly, it is useful to discuss some guidelines which have been adopted in choosing these parameters.

One of the main requirements for observing proton counting, and then consequently, for proton tracking, is that the beam current has to be low enough so that event pile-up is negligible within the shortest exposure time allowed by the detector. As the detector used for these experiments was not designed for particle counting but for integrated imaging, the shortest exposure time achievable with a full frame readout was 153 ms [11]. However, the resulting exposure time was too long for the minimum currents achievable in several experiments (reported in table 1), a trade-off had to be found between the detector area to read and the necessity to image individual protons. For this reason most of the experiments were performed using Regions of Interests (ROIs) in the detector area, as small as 10 rows (or 0.5 mm), to achieve a suitably short exposure time. On the other hand, when the experimental task was to track individual protons, a larger area was needed so that protons scattered in the first detector had a high probability of interacting in the ROI of the second detector and be imaged. A further trade-off between occupancy, i.e. the fraction of detector pixels which detects a proton, and exposure time had to be found.

The parameters used for the experiments of this paper are summarised in table 1.

3 Correlation

The aim of proton tracking is to estimate the probability that two particular events in the two layers are due to the same proton (i.e. to say which proton is which). Capability of proton tracking represents an important requirement in order for CMOS detectors to be used as RT for pCT. However, before effectively trying to track protons, i.e. to identify which proton is which across the DD stack, it is useful to perform a preliminary study of this problem in terms of correlation. The fact that the number of events seen in the two layer shows a good degree of correlation is evidence that the same proton is detected in both layers. This a requirement for protons to be tracked across the two layers. It has to be noted that for the purpose of verifying correlation of number of events detected in two DD layers, timing is of relatively low importance as long as event pile-up is negligible. However, for proton tracking timing, or more specifically readout speed and frame occupancy, will have to be accounted for. In order for proton tracks to be reconstructed across the DD stack, or the full RT, events will have to be sufficiently separated in space to reduce ambiguities and so maintain a sufficient tracking efficiency.

The metric used in this work to assess correlation between the number of events recorded in the two detectors is the *Pearson correlation coefficient*. Given two random variables X and Y, with expected values μ_X and μ_Y and standard deviation σ_x and σ_y respectively, the Pearson correlation coefficient for these two variables $\rho_{X,Y}$ is given by

$$\rho_{X,Y} = \frac{E[(X - \mu_X)(Y - \mu_Y)]}{\sigma_X \sigma_Y} = \frac{cov(X,Y)}{\sigma_X \sigma_Y} \qquad (3.1)$$

where $E[\ ]$ is the expectation value operator and cov( ) is the covariance. A Pearson correlation coefficient of +1 (-1) indicates a perfect direct (inverse) linear relationship. The more $\rho_{X,Y}$ approaches to zero, the more the data are uncorrelated. An advantage of using Pearson coefficient rests in this coefficient being unbiased (i.e. is not sensitive to offsets in the two samples), which is of particular interest for analysis of the DD experiments. In fact, experimental data might be correlated even if not lying on the $x = y$ bisector when one variable is plotted against the other, i.e. with intercept different from zero (due, for example, to higher noise in one detector) and slope different from one (due, for example, to a geometrical efficiency lower than one between the two detectors).

The interpretation to give to the correlation coefficient will depend on the experimental parameters of table 1. As beam and detector geometry, i.e. ROI size, change (see figure 3) the correlation coefficient can be interpreted differently. For Experiments 1, a very small ROI was readout (10 rows or 0.5 mm) when exposed to a large beam (10 cm diameter). Given the small ROI size of this experiment and the large beam area, the ROI readout can be considered as an *equilibrium* region within the larger beam area, where the number of protons seen in the first detector ROI, and scattered outside the second detector ROI, equates the number of protons falling outside the first detector ROI and then scattered inside the second detector ROI. In this case a high correlation coefficient supports the evidence that the number of protons which cross both detector ROIs for each time unit is the same (or proportional depending on the possible different noise level and efficiency of the two detectors). A high correlation coefficient in this experiment will not demonstrate that the same protons are detected in both detectors, as the proton beam spread out from one detector to the other, the probability that the same proton will cross two geometrically corresponding ROIs in the two detectors is low.

The geometry of Experiments 2, 3, 4, 5 is different (see figure 3). In these collimated beam experiments, ROI size is larger than the beam area allowing for protons scattered outside the first detector to still fall within the readout ROI of the second detector. In this case the correlation coefficient can be interpreted differently, related to the probability of seeing the same protons in the two detectors.

3.1 Correlation in uncollimated beam experiments

Data from Experiment 1 are shown in figure 4(a), where the number of events in the downstream detector (*slave*) is plotted against number of events in the upstream one (*master*), for three different values of current (10 nA, 50 nA, 100 nA with a 10^{-2} filter). Although each data group for the various currents spans across a large range of values, a good linear relation is shown between events in the two detectors. The data points of figure 4(a) have an intercept consistent with the x=y bisector, while the slope is lower than one. The slope of this plot can be considered being the efficiency of the DD stack, in fact it

represents the ratio between number of counts in the slave detector and number of counts in the master one.

Figure 4(b) shows ρ over the whole range of currents investigated. Data from Experiment 1 show a good degree of correlation with ρ always greater than 0.8. Given the geometry of this experiment, such a high correlation can be interpreted as a high probability that the number of protons scattered outside the ROI of the second detector is compensated by the a same number of protons scattered inside this ROI. Thus the ROI is effectively in equilibrium.

3.2 Correlation in collimated beam experiments

The same correlational analysis, described in the previous section, was performed on the collimated beam experiments (Experiments 2, 3, 4 and 5 from table 1) to test correlations in experiments where the beam area is fully contained in the ROIs, so that detection of the same protons across the stack can be confirmed. The correlation plot, i.e. counts in the slave versus counts in the master detector is shown in figure 5 for data of Experiment 2 (inset 5(*a*)) and Experiment 4 (inset 5(*b*)), whose experimental parameters described in table 1.

For both experiments shown in figure 5, although counts in both detectors increase with beam current, suggesting evidence of proton counting, data points are circularly distributed for each current value suggesting a poor degree of correlation. For comparison, Pearson correlation coefficient and efficiency is reported in table 2 for all the experiments at iThemba, together with a summary of the experimental parameters used. From table 2, it appears that only Experiment 1, i.e. a small ROI in an uncollimated beam, shows a correlation coefficient high enough to support correlation ($\rho > 0.5$). For all the other collimated beam experiments, regardless of the energy, ρ is often close to zero and the values of efficiency are largely different from experiment to experiment, up to a paradoxical point reached for 5 cm beam experiments where efficiency is greater than 1, showing more counts in the back detector than in the front one.

A direct comparison of the outcomes of the experiments in table 2 is not possible, since many parameters vary from experiment to experiment including the relative beam/ROI geometry, beam current, filtration, exposure time. However, since the efficiency seems to vary substantially across the various experiments, a further investigation into the noise property of the detector is needed.

3.3 Background radiation and SNR

For all the experiments described in this paper a detector threshold T_1 ($T_1 = 19$ DN) was used, equal to three times the noise floor, as measured in dark conditions in the treatment room. However, poorly correlated data in the collimated beam experiments together with a highly variable efficiency resulted in the need to further investigate the noise level in the detectors.

A threshold calculated as described above, is mainly due to detector intrinsic noise and some background radiation in the treatment room, due to relatively long-lived isotopes activated. However, during the actual experiments some additional sources of noise are present, such as secondaries generated in the beam line, in the collimator, in the detector, in the detector

Al back-plates, or secondaries scattered back from the treatment room walls. In order to evaluate this contribution to the detector noise and background radiation, a further dataset was acquired with the beam absorbed in the so called *beam stopper*, a 5 cm thick brass disc to completely stop 191 MeV protons. The number of events measured in dark condition (beam OFF) and with the beam stopper (beam ON + beam stopper) is reported in table 3.

Given the same imaging area and the same exposure time for the two experiments of table 3, the dataset with the beam ON and the beam stopper in place shows a higher number of counts compared to the same data acquired with beam OFF. Also, the efficiency across the stack of two sensors is different for the two experiments: higher for the beam stopper data. These two facts suggest the presence of secondary radiation in the treatment room, and also its anisotropy along the beam direction. This secondary radiation has to be added to the primary signal when the beam is not stopped, and might be responsible for the poor correlation and inconsistent efficiency observed in the collimated beam experiments.

In order to assess the contribution of the secondary radiation to the correlation of the experiments reported in this paper, an analysis of the Signal-to-Noise Ratio (SNR) in terms of noise floor has been performed. The SNR (ratio between number of counts detected and number of counts due to noise) for some of the experiments of table 1 is plotted as function of the nominal beam current in figure 6(a). Two different noise floors are used, either measured with the beam OFF (N_1) or measured with the beam ON and the beam stopper in place (N_2). A line corresponding to SNR = 1 is also plotted for reference. For Experiment 1 data, the SNR is much higher than the nominal limit SNR=1 for both thresholds (ranging from 10^3 to 10^4). However, for collimated beam experiments (Experiment 2 and 4), where the current used is lower and the effective current at the detector plane is further reduced by the geometric efficiency due to the collimator, most data points are barely above the SNR = 1 when the noise floor N_1 is used, and below this line using N_2 as threshold. It can then be deduced from figure 6 how the higher noise level when the beam is ON, due to secondary radiation, leads to a SNR often less than the unity for most of the experiments. This very low figure explains the lack of correlation in the collimated experiments.

To have a measure of the effect of SNR on Pearson correlation coefficient, figure 6(b) shows the value of this coefficient for numerical simulated data[1] with a SNR ranging from 10^{-1} to 10^4 As expected the correlation coefficient increases with SNR, starting from $\rho_{X,Y} = 0.1$ for the lowest SNR value, passing through $\rho_{X,Y} = 0.5$ at SNR = 1 (where there is a 50-50% chance that a generic hit belongs either to the signal or noise distributions), then up to a saturation value of 1 for SNR greater than 70.

From data of figure 6(a), it appears that collimated beam experiments (Experiment 2 and 4) are affected by a low SNR. To try to improve this ratio, it is useful to compare the noise and signal energy spectra to set detection threshold which could further reject noise counts.

---

[1]Numerical simulations were performed by assigning a number of counts to the master sensor, extracted from a Poisson distribution with mean *S*. The number of counts in the slave is assumed to be 90% of the number of counts in the master, to allow for a realistic efficiency. Such data sets result perfectly correlated ($\rho_{X,Y} = 1$). The noise for each SNR value was calculated in order to give the required SNR, where the signal is the sum of the previously calculated signal and noise.

The energy spectra for the beam OFF (N_1), beam ON (N_2) and Experiment 1 (191 MeV) are shown in figure 7(a). It is clear how the three spectra are largely overlapping at this energy, and any attempt to discriminate noise from proton signal based on the signal size is ineffective. However, the lower energy data (30 mm range beam) might offer this possibility since the energy deposition (dE/dx) is higher, helping to distinguish the genuine proton signal from noise and background. For comparison, energy spectra measured in Experiment 1 (191 MeV) and 3 (30 mm range) are shown in figure 7(b). Comparison of these two spectra suggests that using a higher threshold $T_2 = 30$ DN for experiments with the 30 mm range beam (Experiment 3 and 5) can successfully suppress part of the noise, improving the SNR and thus the correlation.

3.4 Correlation in the collimated 30 mm range beam experiments

The 30 mm range beam data appear to be the most suitable of the collimated beam data (see table 1) to verify correlation, since a high threshold can improve the SNR. Figure 8(a) shows the Pearson correlation coefficient for data of Experiment 3 and 5, at the two values of current used, when a threshold based on the detector noise is chosen ($T_1 = 19$ DN) or when a higher threshold, based on the sum of detector noise and background radiation is used instead ($T_2 = 30$ DN). For data of Experiment 3 the use of the high threshold significantly improves the correlation, going from 0.17, at the lowest current using the low threshold, to 0.68 with a high threshold. Similarly for the high current values, $\rho_{X,Y}$ improves from 0.5 to 0.75. However, such an improvement for the second collimated 30 mm range beam (Experiment 5) is not visible. This can be explained by looking at the same quantity (Pearson correlation coefficient), when this is plotted against the SNR estimated for the two experiments (see figure 8(b)). Even when the high threshold is used, figure 8(b) shows how the SNR for Experiment 5 is around 1, resulting in a low correlation, while this values is 2.5 or 7 for Experiment 3, for the two currents used respectively, resulting in a higher correlation.

Hence, when the additional noise sources present in the treatment room are accounted for and the detection threshold is chosen accordingly, collimated experiments with a sufficiently high SNR (Experiment 3) show a significant degree of correlation. Given the geometry of this experiment (see figure 3 and table 1), the high correlation between number of protons seen in the first detector with number of protons seen in the second one, suggest that the same protons are seen in each frame in both detectors, so allowing for proton tracking.

4 Conclusions

The feasibility of using CMOS APSs as energy-range detectors in pCT has been demonstrated by confirming that correlated events are detected in two stacked detectors. An analysis in terms of correlation between events detected in the two stacked CMOS detectors has been performed. For those experiments where a high SNR was achieved, significant correlation was confirmed, suggesting either the evidence of equilibrium regions (in number of events going in and out of the readout ROI) in the beam area or the evidence of same protons being images for the two detectors, depending on the geometry used.

Future work will involve the further development of a proton tracking algorithm to allow to reconstruct proton tracks in the Double DynAMITe stack and in the final PRaVDA range telescope.

Acknowledgments

References

[1]. Smith AR. Vision 20/20: proton therapy. Med Phys. 2009; 36:556. [PubMed: 19291995]

[2]. Yang M, Zhu XR, Park PC, Titt U, Mohan R, Virshup G, et al. Comprehensive analysis of proton range uncertainties related to patient stopping-power-ratio estimation using the stoichiometric calibration. Phys Med Biol. 2012; 57:4095. [PubMed: 22678123]

[3]. Amaldi U, Bianchi A, Chang Y-H, Go A, Hajdas W, Malakhov N, et al. Construction, test and operation of a proton range radiography system. Nucl Instrum Meth A. 2011; 629:337.

[4]. Civinini, C., Brianzi, M., Bruzzi, M., Bucciolini, M., Candiano, G., et al. Towards a proton imaging system. Nucl Instrum Meth A; 1st International Conference on Technology and Instrumentation in Particle Physics; 2010. p. 588

[5]. Sadrozinski, HFW., Johnson, RP., Macafee, S., Plumb, A., Steinberg, D., et al. Development of a head scanner for proton CT. Nucl Instrum Meth A; proceedings of the 8th International "Hiroshima" Symposium on the Development and Application of Semiconductor Tracking Detectors; Academia Sinica, Taipei, Taiwan. December 5–8, 2011; 2013. p. 205

[6]. Schneider U, Besserer J, Pemler P, Dellert M, Moosburger M, et al. First proton radiography of an animal patient. Med Phys. 2004; 31:1046. [PubMed: 15191291]

[7]. [Accessed October 8, 2014] The PRaVDA consortium. 2014. http://www.pravda.uk.com

[8]. Taylor JT, Allport PP, Casse GL, Smith NA, Tsurin I, Allinson NM, et al. Proton tracking for medical imaging and dosimetry. JINST. 2015; 10 C02015.

[9]. Poludniowski G, Allinson NM, Anaxagoras T, Esposito M, Green S, Manolopoulos S, et al. Proton-counting radiography for protontherapy: a proof of principle using cmos aps technology. Phys Med Biol. 2014; 59:2569. [PubMed: 24785680]

[10]. Esposito M, Anaxagoras T, Fant A, Wells K, Konstantinidis A, Osmond JPF, et al. DynAMIte: a wafer scale sensor for biomedical applications. JINST. 2011; 6:C12064.

[11]. Esposito M, Anaxagoras T, Konstantinidis AC, Zheng Y, Speller RD, Evans PM, et al. Performance of a novel wafer scale cmos active pixel sensor for bio-medical imaging. Phys Med Biol. 2014; 59:3533. [PubMed: 24909098]

[12]. Scheffer D. A wafer scale active pixel cmos image sensor for generic x-ray radiology. Proc SPIE. 2007; 6510:65100O.
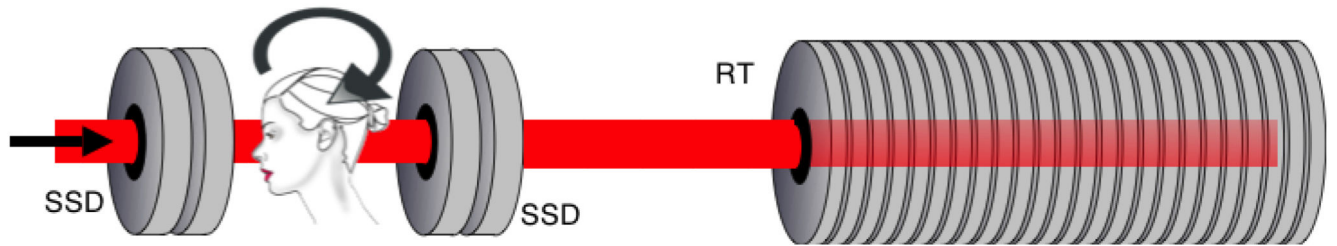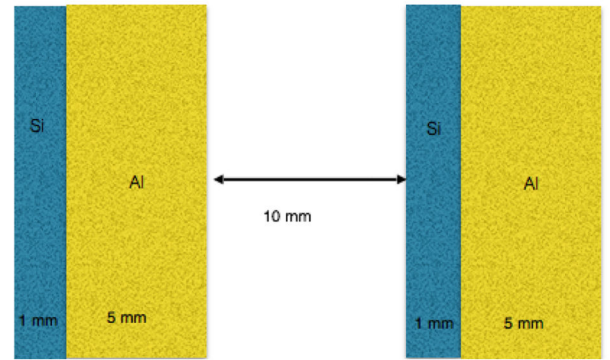
Figure 1.
A schematic representation of the proposed PRaVDA system for pCT. Two sets of three Silicon Strip Detectors (SSD) are placed before and after the patient, to infer protons most likely path through the patient. A stack of CMOS APSs (RT) is placed after the patient, to record the protons residual energy.
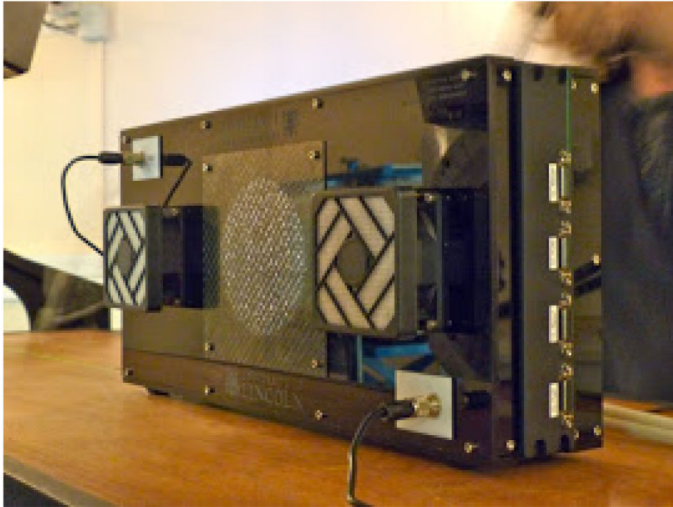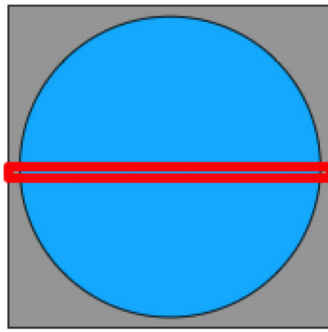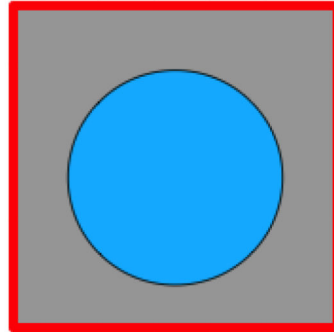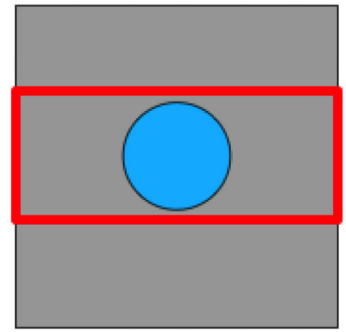
(a)

(b)

Figure 2.
a) The DD set-up during experiments at iThemba. An optical collimation tool is used to project the beam area on the detectors. The stack of detectors is placed at iso-centre on a treatment coach. *b*) A schematic showing the configuration of the DD set-up.

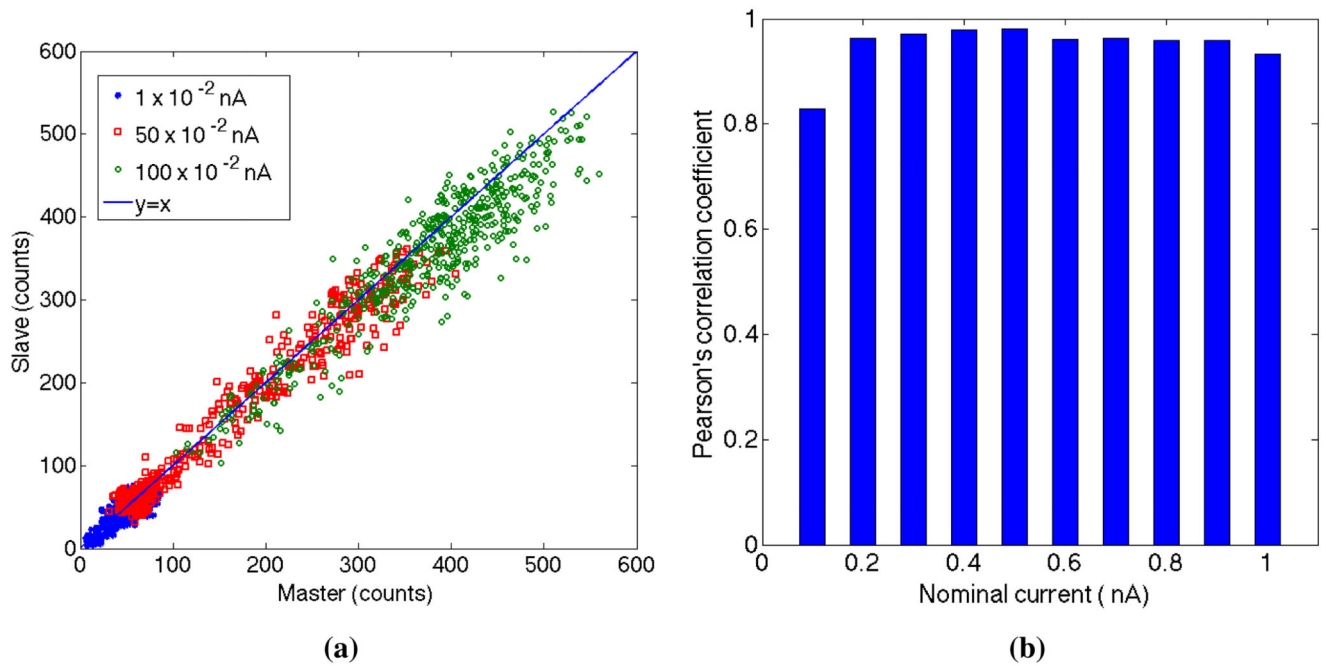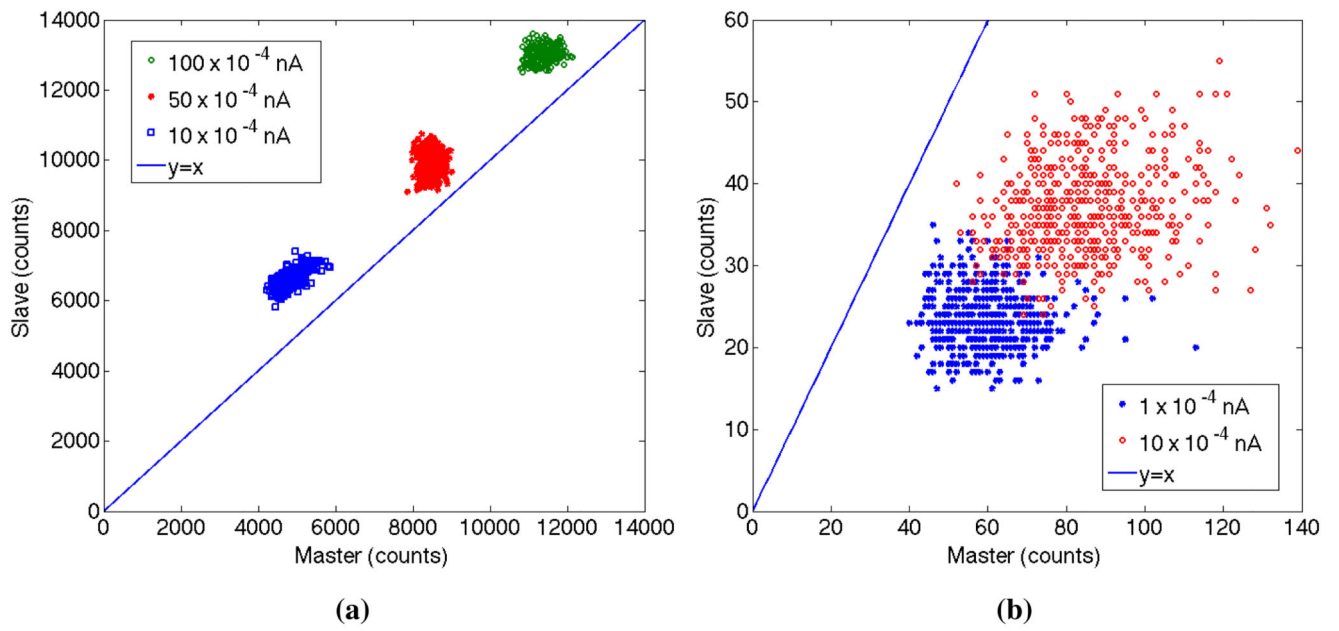**Figure 3.**
Schematic representation of the beam and detector geometry for the iThemba experiments. Blue circles represent the beam area, the red regions highlight the ROIs readout over the whole detector area (grey area).
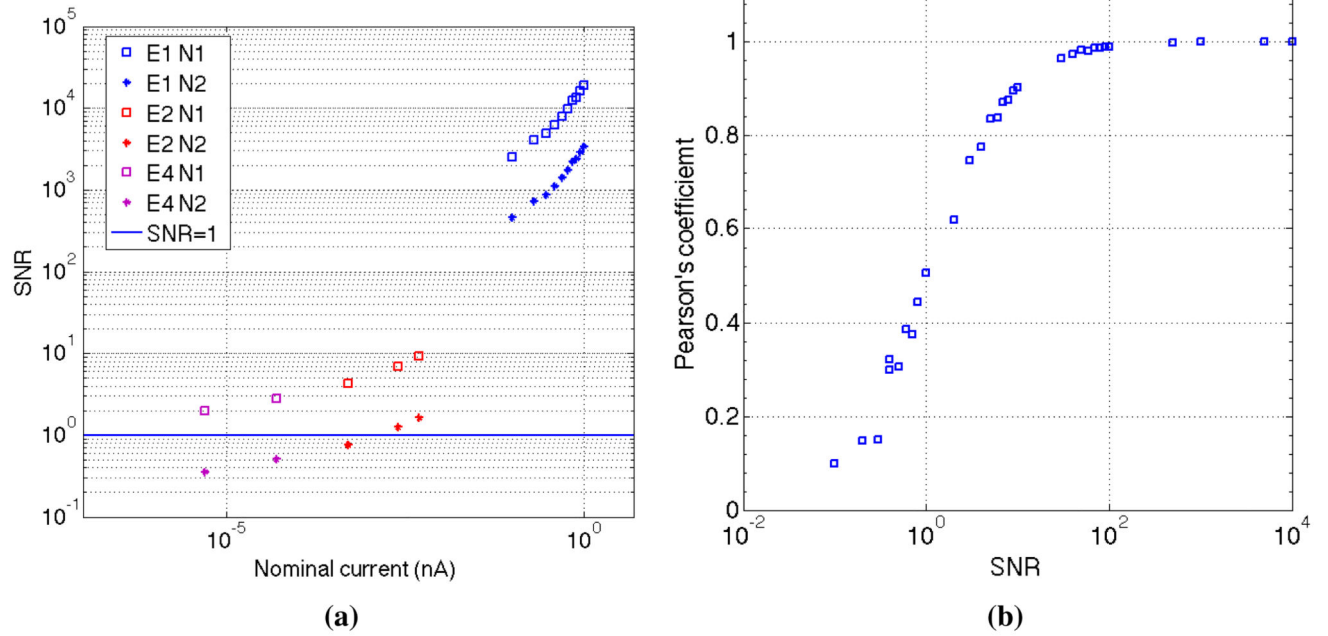
Figure 4.

a) Number of events detected in the slave for each frame as a function of number of events in the master, for some values of the beam current. The $x = y$ bisector is also shown. *b*) Pearson correlation coefficient for data of Experiment 1.

(a)

(b)

Figure 5.
Number of counts in the slave detector plotted against the number of counts in the master one for data of Experiment 2 (*a*) and 4 (*b*). The *x* = *y* bisector is also shown.

(a)

(b)

Figure 6.
a) SNR calculated for Experiments 1 (E1), 2 (E2) and 4 (E4) when the noise is calculated with the beam OFF is considered (N_1) or with the beam ON and the beam stopper in place (N_2). A reference line corresponding to SNR = 1 is also shown. *b)* Pearson correlation coefficient, obtained by numerical simulated data, as a function of SNR.

(a)

(b)
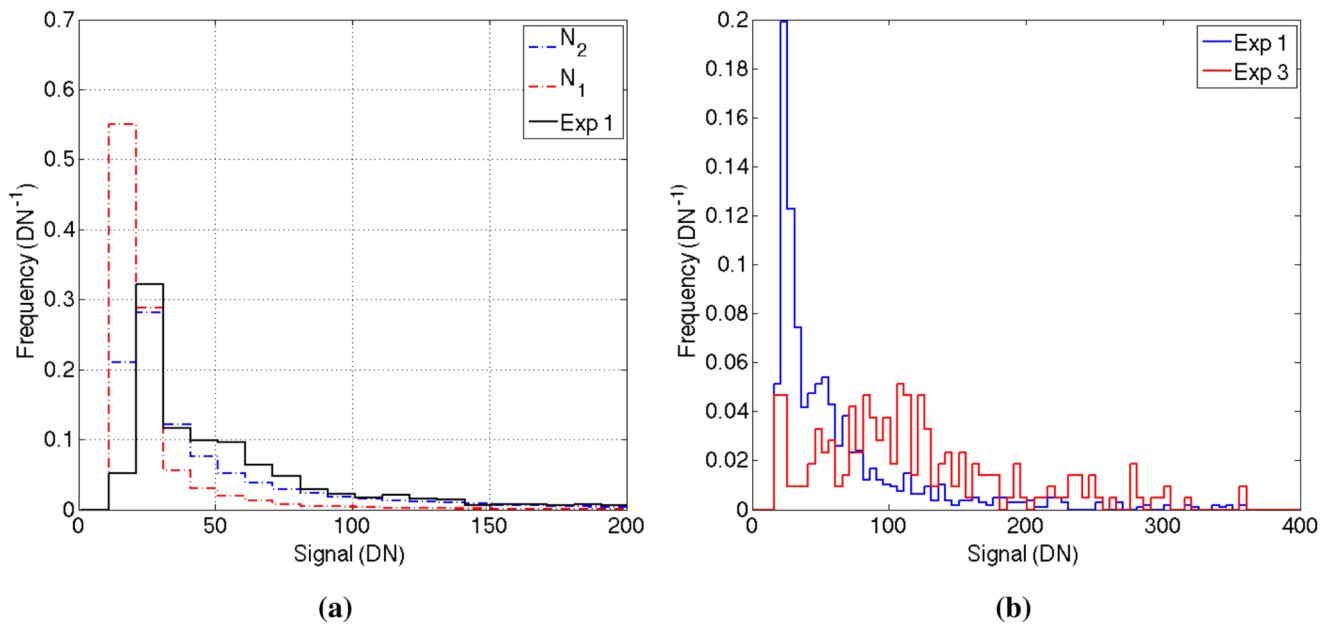
Figure 7.
a) Energy spectra measured with the beam OFF (N_1), with the beam ON and the beam stopper in place (N_2) and with 191 MeV protons (Experiment 1). *b*) Energy spectra measured at 191 MeV (Experiment 1) and for the 30 mm range beam (Experiment 3).

(a)

(b)
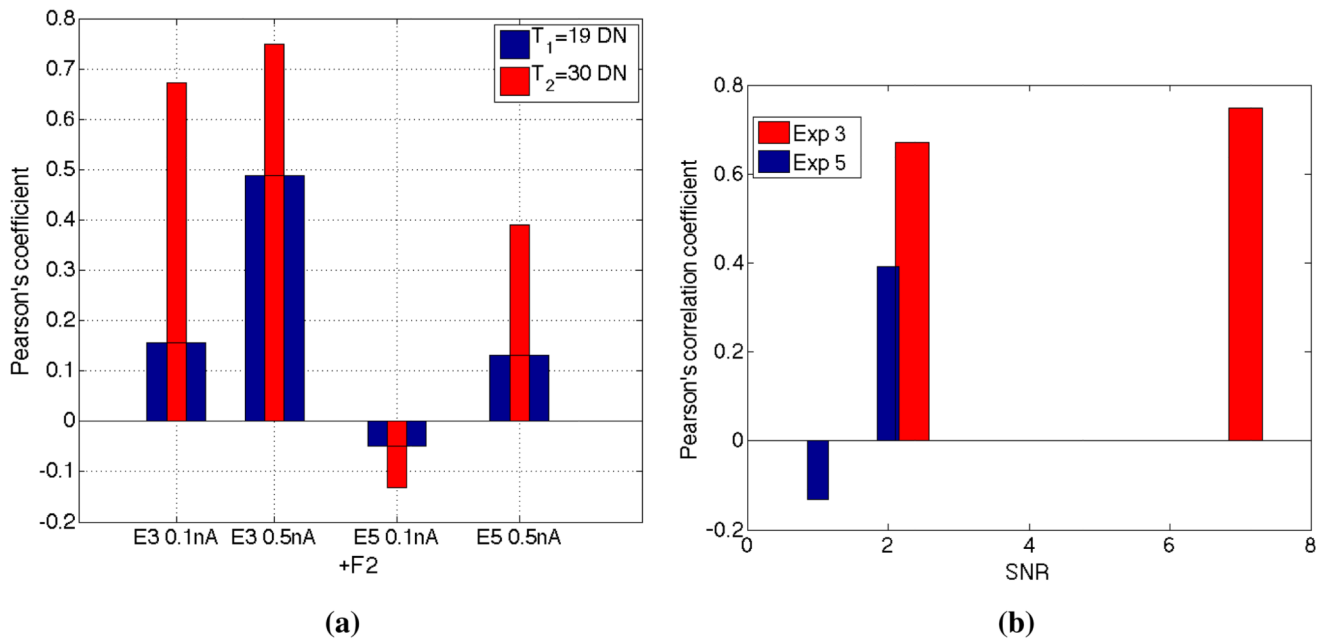
Figure 8.
a) Pearson correlation coefficient for Experiment 3 and Experiment 5 when a threshold based on the detector noise is used ($T_1 = 19$ DN), or when a threshold based on the detector noise and background radiation is used ($T_2 = 30$ DN). *b*) Pearson correlation coefficient for Experiment 3 and 5 plotted against SNR, with a threshold of 30 DN.

Table 1

Experimental parameters used at the iThemba proton facility. The ROI used is specified here only as a number of rows, as the number of columns to readout was fixed (2520 columns). The value of current reported was the beam current before applying the 10^{-2} or 10^{-4} filter. The beam range is measured as 50% of maximum dose on the distal side of the Bragg peak in water. The ratio between the ROI area and the beam area is also reported, showing the fraction of beam contained in the ROI. With the exception of Experiment 1, this figure is greater than one implying that all protons are detected in the ROI.

Experiment number	Energy MeV	Range mm	Current nA	Filter	Beam size cm	A_{ROI}/A_{beam}	Rows	Exp time ms
1	191	240	10-100	10^{-2}	10	0.1	10	0.76
2	191	240	10, 50, 100	10^{-4}	5	164	2560	153
3	60	30 mm	0.1, 0.5	10^{-2}	5	164	2560	153
4	191	240	1, 10	10^{-4}	0.5	2567	400	24
5	60	30 mm	0.1, 0.5	10^{-2}	0.5	2567	400	24

Table 2

Pearson correlation coefficient and efficient, namely the ratio between counts in the slave and counts in the master, for all the experiments performed at iThemba together with a summary of the experimental parameters used.

Experiment number	Energy MeV	Current nA	Filter	Beam size cm	Rows	Exp time ms	Pρ	Efficiency
1	191	10	10^{-2}	10	10	0.76	>0.83	>0.9
2	191	10	10^{-4}	5	2560	153	0.72	1.4
2	191	50	10^{-4}	5	2560	153	0.05	1.2
2	191	100	10^{-4}	5	2560	153	0.18	1.1
3	60	0.1	10^{-2}	5	2560	153	-0.12	1.9
3	60	0.5	10^{-2}	5	2560	153	-0.79	1.5
4	191	1	10^{-4}	0.5	400	24	-0.02	0.4
4	191	10	10^{-4}	0.5	400	24	0.20	0.4
5	60	0.1	10^{-2}	0.5	400	24	-0.05	0.4
5	60	0.5	10^{-2}	0.5	400	24	-0.13	0.3

Table 3

Counts in master and slave and their ratio, efficiency, for full frame ROI images acquired with the beam OFF or with the beam ON and stopped with the brass beam stopper.

	ROI	Current nA	Master counts	Slave counts	Efficiency
Beam OFF	2560×2520	0	4500	1930	0.43
Beam Stopper	2560×2520	0.4	6450	9030	1.4